Rationally Designed Complex, Hierarchical Microarchitectures
Wim L. Noorduin *et al.*
Science **340**, 832 (2013);
DOI: 10.1126/science.1234621

Science (print ISSN 0036-8075; online ISSN 1095-9203) is published weekly, except the last week in December, by the American Association for the Advancement of Science, 1200 New York Avenue NW, Washington, DC 20005.

Rationally Designed Complex, Hierarchical Microarchitectures

Wim L. Noorduin,[1]* Alison Grinthal,[1] L. Mahadevan,[1,2,3,4] Joanna Aizenberg[1,2,3,5]*

The emergence of complex nano- and microstructures is of fundamental interest, and the ability to program their form has practical ramifications in fields such as optics, catalysis, and electronics. We developed carbonate-silica microstructures in a dynamic reaction-diffusion system that allow us to rationally devise schemes for precisely sculpting a great variety of elementary shapes by diffusion of carbon dioxide (CO_2) in a solution of barium chloride and sodium metasilicate. We identify two distinct growth modes and show how continuous and discrete modulations in CO_2 concentration, pH, and temperature can be used to deterministically switch between different regimes and create a bouquet of hierarchically assembled multiscale microstructures with unprecedented levels of complexity and precision. These results outline a nanotechnology strategy for "collaborating" with self-assembly processes in real time to build arbitrary tectonic architectures.

Natural patterns and shapes arise in innumerable ways on a range of scales and have fascinated artists and scientists alike (*1*, *2*). Hierarchical nano- and microarchitectures not only offer insight into how complex forms can emerge from simple starting materials, but also underlie coloration (*3*), wetting (*4*), mechanics (*5*), and other phenomena seen in nature and may transform optics (*6*), catalysis (*7*–*9*), building construction, and many other technologies if we can find ways to create them synthetically. Using top-down lithography techniques (*10*), we can directly write and sculpt three-dimensional (3D) patterns into a variety of materials, but at small scales this hands-on control translates into a laborious, costly, and often insufficient approach. Self-assembly from the bottom up can generate diverse patterns through a much more complex evolution of forces than we could ever apply by hand (*11*); however, ceding control over all but the starting materials leaves little opportunity to fine-tune structures or control stages of hierarchical development, let alone rationally design arbitrary architectures. Strategies inspired by biomineralization have been explored as potential routes to controlling growth and self-assembly from the molecular level via tailored microenvironments, epitaxy, and inorganic or organic additives (*12*–*21*). Yet although these strategies have produced some interesting spherical, spiral, leaflike, and other shapes (*22*–*29*), the appearance of various forms in synthetic systems is often unexpected and not usually based on predictive mechanisms.

The vast majority of efforts to apply biomineralization principles to synthetic strategies have, like most nanoscale self-assembly techniques, focused primarily on defining the initial conditions or solution composition. Although this approach has certainly yielded useful insights, it is obvious that many complex patterns emerge specifically in response to a dynamic environment. For example, abrupt switches in marine shell patterning have been attributed to changes in conditions during growth (*1*); at a larger scale, bacteria form hierarchically structured communities by chemotactically responding to continuously changing chemical cues (*30*). This perspective not only highlights a major source of complexity and hierarchy currently missing from synthetic strategies, but also suggests that we might be able to actively shape self-assembling structures by manipulating the environment as they grow. This possibility is especially compelling for systems that develop through reaction-diffusion processes, where dynamic feedback between the reaction front and the solution is the central mechanism of pattern evolution (*31*–*35*). Such feedback mechanisms are not only proposed to explain a variety of natural forms, but they can also generate patterned precipitation in synthetic systems (*36*). We therefore explore whether mineralized forms can be precisely sculpted and hierarchically assembled into novel, arbitrary architectures through dynamic, rationally programmed modulations of the reaction solution.

In this work, we demonstrate how the responsive growth of $BaCO_3$-SiO_2 structures toward or away from the bulk solution can be exploited to program a variety of "elementary" growth patterns. We derive sequences of simple, subtle modulations of CO_2, pH, and temperature that serve as building strategies for intricate, user-defined microstructures of higher order. With the use of continuous and/or stepwise adjustments, we steer the precipitating reactants via precise sculpting and sequential combinatorial assembly of the developing shapes.

Hypothesis for Structure Evolution in a Field of Chemical Gradients

Our strategy for dynamically modulating structure evolution is based on the idea that the developing structure will be continuously shaped by a complex spatial field of overlapping chemical gradients, created by the interplay between the bulk solution, the reaction front, and potentially neighboring structures. We analyze this

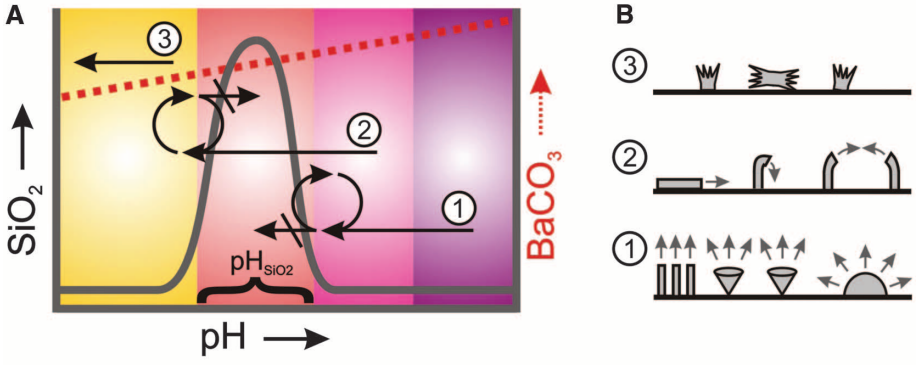

Fig. 1. Hypothesis for structure evolution in three growth regimes. Schematic representation of the rate of SiO_2 (*37*) (solid gray line) and $BaCO_3$ precipitation (dashed red line) in the range of pH ~8 to 12 (**A**) and anticipated shapes and growth directions (**B**) resulting from the three proposed growth regimes (see text for details). In all cases, growth will begin with the nucleation of $BaCO_3$, which will lead to the local reduction of pH at the growth front. In regime 1, the associated pH drop brings the structures to the right side of the silica deposition range (denoted as pH_{SiO2}), giving rise to the continuous coprecipitation of $BaCO_3$ and SiO_2. The structures will grow most successfully away from one another and toward the solution where $pH > pH_{SiO2}$, whereas other growth directions associated with lower pH become passivated by silica. Depending on the nucleation density, we expect the structures to "blossom" into stems, cones, and hemispherical shapes. In regime 2, the pH drop from carbonate deposition will lower the pH at the growth front to $pH < pH_{SiO2}$, whereas the bulk solution remains more alkaline with $pH > pH_{SiO2}$. In this case, any growth directions toward the higher pH bulk solution will cross the silica precipitation region and be blocked, such that the structures are expected to grow most successfully away from the solution, along the interface, or curl down and toward each other where pH remains below pH_{SiO2} following the trail of produced acid. In regime 3, only $BaCO_3$ crystals are expected to form.

[1]School of Engineering and Applied Sciences, Harvard University, Cambridge, MA 02138, USA. [2]Wyss Institute for Biologically Inspired Engineering, Harvard University, Boston, MA 02115, USA. [3]Kavli Institute for Bionano Science and Technology, Harvard University, Cambridge, MA 02138, USA. [4]Department of Physics, Harvard University, Cambridge, MA 02138, USA. [5]Department of Chemistry and Chemical Biology, Harvard University, Cambridge, MA 02138, USA.

*Corresponding author. E-mail: wnoord@seas.harvard.edu (W.L.N.); jaiz@seas.harvard.edu (J.A.)

growth process for the coprecipitation of SiO_2 and $BaCO_3$ in an alkaline aqueous solution containing Na_2SiO_3 and $BaCl_2$, where precipitation is triggered by the diffusion of CO_2. $BaCO_3$ deposition increases with increasing pH, whereas SiO_2 deposition takes place in a narrow, optimum pH_{SiO2} range (Fig. 1A) (*37*), and mutual feedback between the two processes may create a reaction-diffusion scenario. We hypothesize that the pH-dependent feedback between $BaCO_3$ and SiO_2 deposition will lead to three distinct growth regimes, each with a characteristic set of morphologies, which can be evoked by small changes in the environment, as follows:

Regime 1) Starting with a high-pH bulk solution (region 1 in Fig. 1A), no silica deposition will take place, and the influx of CO_2 will trigger the precipitation of $BaCO_3$, according to a simplified reaction: $Ba^{2+} + CO_2 + H_2O \rightarrow BaCO_3 + 2H^+$. The released H^+ will gradually lower the local pH at the growth front, until entering the pH range for silica precipitation, according to a simplified reaction: $SiO_3^{2-} + 2H^+ \rightarrow SiO_2 + H_2O$, which then shifts the reaction equilibrium and solubility back toward $BaCO_3$ precipitation, resulting in the continuous coprecipitation of $BaCO_3$ and SiO_2 (*25*). This scenario will have several consequences for the developing structure: (i) Crystal growth will be passivated where silica precipitates, (ii) structures should grow most successfully toward the bulk solution where pH is above the range for silica deposition, and (iii) growth should be inhibited near the lowered pH of neighboring growth fronts. Depending on the nucleation density, different basic morphologies might then be expected: hemispheres at low nucleation densities, or cones and stem shapes at higher densities, where neighboring diffusion fields steer the structures away from each other toward regions of higher pH (Fig. 1B).

Regime 2) Lowering the initial bulk pH can generate a scenario in which the local pH is below the optimum pH for silica formation (pH_{SiO2}), whereas the bulk pH is still above pH_{SiO2} (region 2 in Fig. 1A). In this case, the local decrease in pH due to continuing $BaCO_3$ crystallization prevents, rather than promotes the formation of SiO_2 close to the growth front, whereas the influx of the bulk solution with $pH > pH_{SiO2}$ brings the solution into the pH_{SiO2} range and triggers the precipitation of SiO_2 that passivates growth. Structures will then be expected to grow most successfully away from the bulk solution, either along the interface to form flat sheets or curling down and toward each other to preserve a low pH at the growth front (Fig. 1B).

Regime 3) If the pH of the bulk solution is below the pH_{SiO2} range, only "normal" $BaCO_3$ structures should form (region 3, Fig. 1).

Testing Regime 1: Solution-Directed Growth of Stems, Vases, and Corals

As a first step toward testing the solution-dependent growth of structures in regime 1, we created a gradient of CO_2 concentrations by vertically positioning an aluminum plate or gold-coated glass substrate in a beaker containing an aqueous solution of $BaCl_2$ (19.1 mM) and Na_2SiO_3 (8.2 mM) at a pH of 11.8 and loosely covering the beaker to let CO_2 from the air diffuse into the system (Fig. 2A). The nucleation density of $BaCO_3$, gradually decreases with depth, in accord with the decrease in CO_2 concentration. Within 2 hours, the nucleated $BaCO_3$ bundles develop into a dense forest of thin stems at the top of the substrate, where the CO_2 concentration is highest (Fig. 2A and fig. S1). At intermediate depths, the structures instead become vaselike and form coral-like hemispherical shapes toward the bottom. In all cases, the structures grow perpendicular to the substrate—that is, toward the bulk solution where $pH > pH_{SiO2}$—and veer away from each other. The basic morphologies and behavior are, thus, consistent with the solution-directed growth hypothesis proposed for regime 1. Yet at the same time, the intricate wall structures observed in the vases and corals provide another level of complexity within each of the basic shapes, supporting the idea that this growth mechanism also contains the seeds for more complex modulations.

Inspection by scanning electron microscopy (SEM) reveals that the walls have a constant thickness of ~1 μm, with a consistent thickening of stems and at the edges of the walls (Fig. 2B). The constant wall thickness suggests a 2D growth mechanism, in which precipitation merely occurs at the active top edges of the structures while being inhibited by silica at the sides. Selective dissolution of $BaCO_3$ using HCl (0.5 mol/L) leaves behind a hollow silica shell (fig. S2), further indicating that the silica mainly deposits on and selectively passivates the sides of the walls where the pH is lowest (Fig. 2C). This localized silica precipitation sets the thickness of the walls because the pH in the middle of the growth front is less buffered than closer to the sides where silica precipitation mainly occurs, allowing a new layer of $BaCO_3$ crystals to grow at the top of the walls. The increased thickness at the edges of the walls and stems is also consistent with solution-directed growth: These areas have a larger surface to accommodate the silica deposition, resulting in local thickening (Fig. 2B). The localized feedback also produces a uniform 2D growth front by dampening the formation of spontaneous protuberances. To directly demonstrate that the structures evolve toward the highest pH, we grew them in a continuous flow that increased the pH at the growth front using a microfluidic device. The

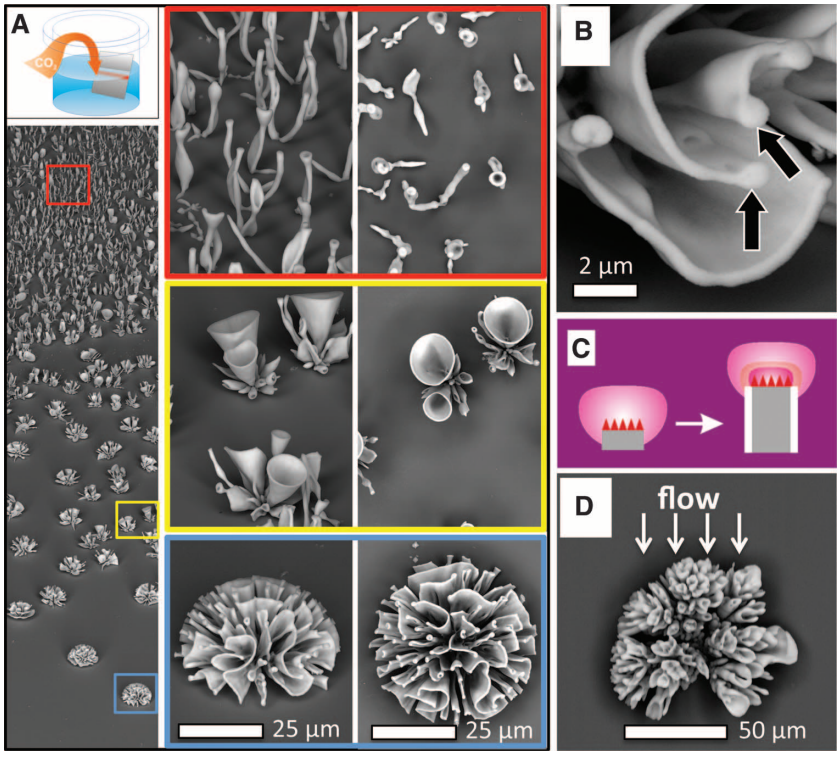

Fig. 2. Diversity of structures that grow in regime 1. (**A**) SEM image of a typical substrate vertically submerged in solution with an initial bulk pH of 11.8, showing a gradient of shapes (from top to bottom of the substrate: 1D stems, conical vases, and hemispherical coral-like structures). The enlarged side and top views of the structures in the red, yellow, and blue boxed regions are shown on the right. (**B**) High-magnification SEM image of a coral structure, showing the thickening of the sides of the walls (indicated by arrows). (**C**) Schematic of a 2D growth mechanism, in which the thickness of the walls and stems is fixed by the short-range buffering action of silica deposited on the walls (shown in white) that locally increases pH at the $BaCO_3$ growth front (the color scheme matches that in Fig. 1). (**D**) Top view of the coral structure grown in a flow in a microfluidic reactor. Directional growth toward the flow, where the pH is highest, is observed, consistent with the solution-directed growth behavior.

structures primarily grow against the flow along the interface (Fig. 2D), in the direction of the high-pH bulk solution.

This basic, relatively simple directed growth behavior thus enables both straightforward selection and continuous sculpting of the evolving structures into a diversity of well-controlled forms. For example, the wall thickness can be dynamically modulated by increasing and decreasing the flux of CO_2. A temporary increase in CO_2 was imposed by opening the lid of the beaker, resulting in a thickening of the walls due to the increased carbonate deposition (Fig. 3A and fig. S3). This thickening occurs only at the growth edge, and the original wall and stem thickness is rapidly restored by the feedback mechanism when the lid is placed back on. As the growth rate is constant, we are able to use rhythmical fluctuations in the CO_2 concentration to produce well-defined series of ripples (Fig. 3B). This control over wall thickness further provides the means to prescribe the splitting and branching of the growth front. Specifically, if the wall thickness exceeds a critical size, the center of the growth front will not be sufficiently buffered by the silica deposition at the sides to continue growing, leading to a complete breakup of the growth front into new, separate growth fronts that branch away from each other (Fig. 3C). To reach such increased thicknesses, we performed experiments using $SrCO_3$ in place of $BaCO_3$. $SrCO_3$ yields the same set of morphologies, but because its solubility is half that of $BaCO_3$, a similar CO_2 pulse results in the precipitation of more carbonate and leads to a substantially greater thickening of the wall, inducing stems to open out into uniform vases (Fig. 3D). Perturbation of the thickness of the growth front by increased carbonate deposition can, thus, be swiftly restored to the original dimension by either slimming (Fig. 3A) or complete splitting of the front (Fig. 3C), depending on the precise magnitude of the perturbation.

In addition to directly modulating CO_2 or replacing $BaCO_3$ with $SrCO_3$, the structures can also be finely sculpted by controlling the temperature or salt concentration of the bulk solution. Lowering the temperature provides an alternative means to increase the amount of available CO_2, and we indeed observe a thickening of the walls (while preserving the overall shapes of the stems, vases, and corals) by simply cooling the solutions to 4°C (Fig. 3E). Adding NaCl increases the silica deposition rate (*38*) but leaves the $BaCO_3$ crystallization virtually unaffected (fig. S4). Again, this leads to a thickening of the walls to give similar structures, as shown in Fig. 3E. A variety of simple continuous modulations in the bulk solution can thus be used to dynamically steer the shape of the growing structures, allowing multiple levels of controlled sculpting.

Testing Regime 2: Further Diversity Through Inward-Directed Growth

When we shift to regime 2 by lowering the pH of the bulk solution to 11.2, we observe an entirely different collection of shapes (Fig. 4A) (*39*). The basic shapes—including single and double spirals, as well as globular and leaflike structures—are consistent with the curling mode of growth and resemble those reported previously (*25*–*28*). In contrast to the pronounced gradient of structural variation observed in regime 1, here even a single set of bulk conditions gives rise to a tremendous diversity of forms that not only grow next to each other, but even appear together as part of composite structures. This diversity can be explained by considering how structures grow to avoid the passivating pH_{SiO2} range: Whereas in regime 1 the structures grow toward the bulk solution, where $pH > pH_{SiO2}$, and away from neighbors, in regime 2 their growth appears inward, away from the bulk solution and toward their own and neighboring growth fronts, where $pH < pH_{SiO2}$. In direct support of this mechanism, structures growing in a microfluidic reactor at pH 11.2 point away from the bulk solution (Fig. 4B), developing in the direction opposite that observed in regime 1 (Fig. 2D). This inward-directed growth can be expected to make the emerging shapes highly sensitive to small variations in local diffusion fields, driving a more intricate chemical

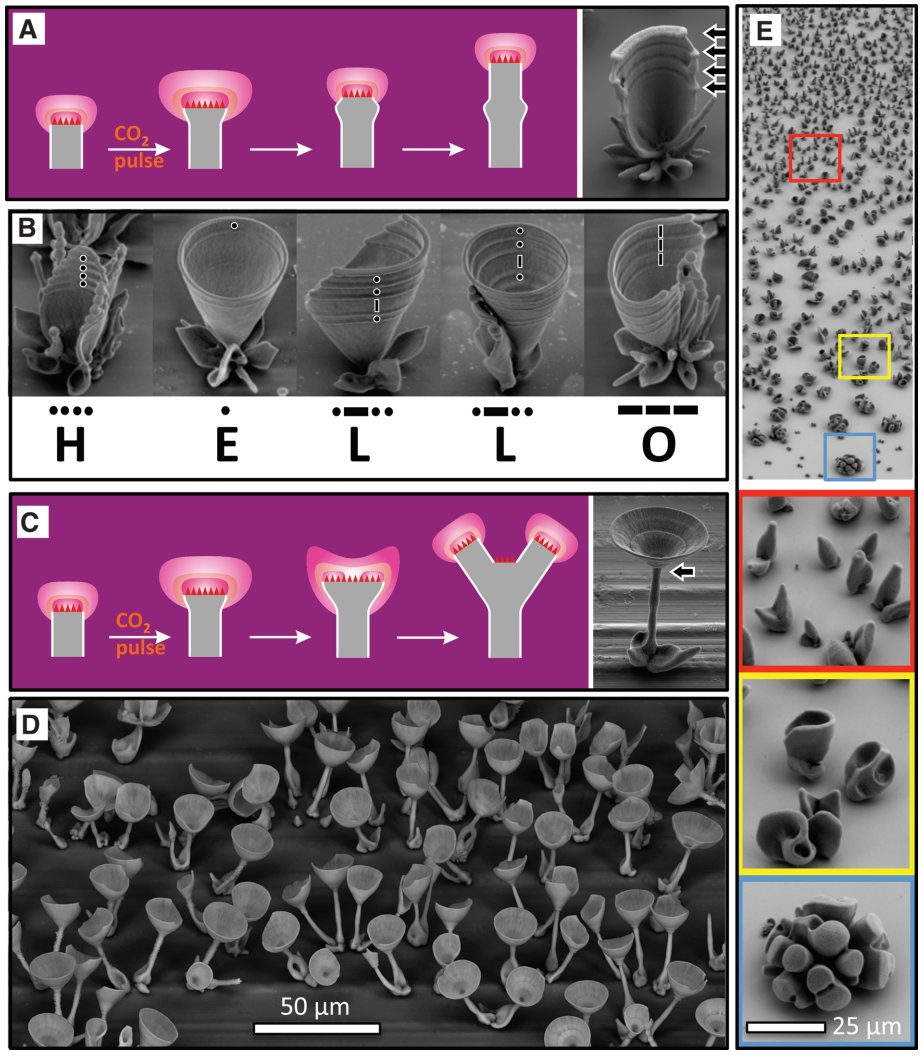

Fig. 3. Dynamically sculpting the growing stems, vases, and corals. (**A**) Schematic of the mechanism of restoration of the original, well-defined wall thickness after a temporary increase of the wall thickness is induced (by, for instance, a pulse of CO_2). The colors correspond to the pH regions in Fig. 1. (**B**) Experimental demonstration of (A). Rhythmical pulsing of CO_2 in the Ba-Si solution controllably produces ripples in the growing structures that can be used to write messages in Morse code. The "L" structures are from the same experiment; the other letters are made in separate experiments. (**C**) Schematic of the proposed mechanism of the splitting of the growth front to restore the original dimension, when the temporary increase of the wall thickness exceeds the dimension of the buffering front established by silica on the side walls. The arrow indicates a splitting point. (**D**) Experimental demonstration of splitting using a pulse of CO_2 into a Sr-Si solution, allowing sculpting stems into vases. (**E**) The structures can also be thickened, while preserving the overall morphologies, by increasing either the availability of CO_2 or the rate of the silica precipitation, which are achieved by lowering of the temperature (shown) or addition of NaCl, respectively.

interplay between nearby structures and different regions of their own surfaces.

The simultaneously appearing basic shapes can each be understood by the inward-directed growth that characterizes regime 2 (Fig. 4, C to F; see fig. S5 for details): (i) Large leaflike structures covered with a mantle of silica (Fig. 4C) arise when the nucleated $BaCO_3$ crystals grow along the substrate, where the pH in the vicinity of the growth front remains sufficiently low ($pH < pH_{SiO2}$) to prevent passivation by silica precipitation, whereas silica deposition occurs on top of the structure due to the flux of a more basic solution from the bulk. (ii) Single spirals form in response to perturbation of the growth front of the nucleated $BaCO_3$ crystals that results in a lower pH at one side of the front and a higher pH at the opposite side. The lowering of the local pH causes two complementary effects: growth toward the lower pH to remain in the region of $pH < pH_{SiO2}$ and, conceivably, a slightly decreased $BaCO_3$ growth rate on the inner side of the curved structure. As the outer part continues growing and is passivated by silica, this further shields the inner part from the bulk solution, lowering the local pH inside even more. The structure will continue to curl in this direction to give an increased curvature until the front is hampered by its own tail (Fig. 4D). To visualize this initial curling, we developed a method to grow quasi-2D structures by pinning the meniscus on the substrate (Fig. 4G). If we allow the structures to grow in 3D, the growth front continues to curl in the same direction, thereby following the acid that is produced by the previously formed part of the structure and generating a single spiral. This underlying part also shields the growth front from the bulk solution, comparable to the manner in which the substrate promotes growth of the leaves. (iii) Double spirals emerge when, instead of following its own tail, a growth front bends in the direction of the acid produced by a nearby $BaCO_3$ growth front. In this case, the two active sites follow each other's tails, making a double spiral (Fig. 4E). To confirm this cooperative growth mechanism, we grew a dense field of structures in regime 1 and subsequently lowered the pH to the curling growth mode. As can be observed from Fig. 4, H and I, the structures, which first grow away from each other and into the solution in regime 1, begin to "sense" each other's active growth fronts, grow toward each other and away from the bulk, and finally merge to form single and double spirals in regime 2, in agreement with the hypothesis presented in Fig. 1. When one of the growth fronts of the double spiral catches up with the other one, they combine to form a single spiral with preservation of the chirality (Fig. 4, A and E). (iv) Finally, globular structures can be formed when two growth fronts crash into each other and merge together to become completely passivated by silica (Fig. 4F). The abundant acid that is released produces a local thickened scar on the silica mantle found on most globular structures (Fig. 4A).

The formation of spirals, double spirals, leaves, and globular shapes can thus be explained by growth-induced localized acid formation, which lowers the pH below the range for silica precipitation that passivates the growth, inducing structures to (i) grow most successfully away from the bulk solution and toward each other and (ii) curl as a result of the nonuniform growth rates that arise from the pH-dependent solubility (*40*). It is important to note that this mechanism can

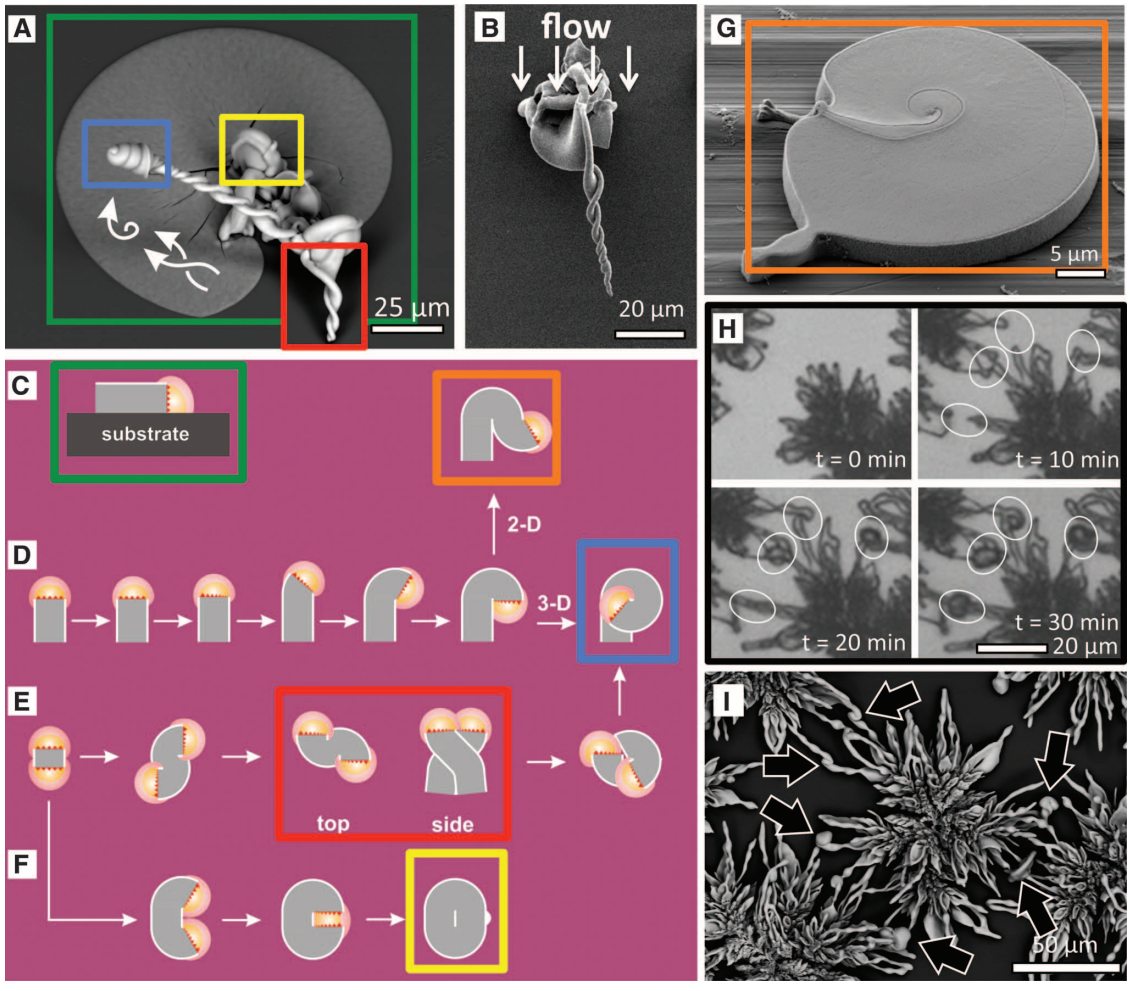

Fig. 4. Diversity of structures that grow by inward-directed growth in regime 2. (**A**) SEM image of an exemplary $BaCO_3$-SiO_2 structure grown at pH 11.2 containing a single spiral (blue rectangle), a double spiral (red rectangle), leaf shapes (green rectangle), and globular shapes (yellow rectangle). (**B**) Top view of a spiral grown in a flow, demonstrating directional growth away from the flow of bulk solution. (**C**) Leaflike structures grow along the interface, away from the solution and become passivated on the top by a silica mantle. (**D** to **F**) Mechanisms of three curling modes, in which the structures curve away from the bulk solution and follow the trail of the acid produced at their own or neighboring growth fronts, resulting in the formation of single (D) and double (E) spirals and globular (F) structures (see text and supplementary materials for details). (**G**) Demonstration of the curling mode in a thin film of the solution that allows meandering only in 2D and eventually ceases when crashing into its own tail. (**H** to **I**) Optical microscopy time lapse series of a dense field of structures that initially (time $t = 0$ min) steer away from each other in regime 1 and then grow toward each other and merge upon lowering the pH to regime 2 to create spirals, as indicated by arrows in (I).

account for the full richness of observable forms and that it is principally different from a mechanics mechanism previously proposed to explain spiral formations (*25*).

Beyond Basic Shapes: Hierarchical Combinatorial Architectures

Because the morphology of the growing structures is responsive to the solution conditions and independent of the underlying form, a wide variety of different shapes can be stacked on top of each other by controlling the position, pH, temperature, and salt concentration in serial growth steps that distinctly allow for the formation of diverse higher-order architectures assembled hierarchically from the elementary building blocks. Here, we provide only a few exemplary cases to illustrate the concept (Fig. 5 and figs. S6 to S8). When structures are grown sequentially in two different growth solutions, the second precipitation takes place preferentially at the active barium or strontium carbonate growth sites of the already-existing structures, showing no overgrowth of silica-passivated surfaces. We illustrate this by comparing the same structures before and after the second growth using SEM and confocal microscopy of dyed solutions (Fig. 5, A to C). By simply positioning the substrate at an angle relative to the first growth, we create a combinatorial matrix of reaction conditions that yield a large structural diversity with regions exhibiting well-defined hierarchical shapes on a single sample (Fig. 5D). When the structures grown in the first step become overcoated with SiO_2, these sites are passivated, so that the only nucleation sites available for the second precipitation are hidden in the cavities of the structure where the growth fronts split (Fig. 5, E and F). When the pH of the solution is reduced during the experiment from regime 2 to regime 3, spiral formations become overgrown by pure $BaCO_3$ bundles (Fig. 5G). Additionally, patterned substrates can be selectively decorated with structures (Fig. 5H). In all cases, the sculpted complex architectures show an unprecedented level of structural uniformity over large areas (see representative examples in Fig. 3D; Fig. 5, E and F; and figs. S6 to S8). Thus, the separate growth steps make it possible to create combinatorial, hybrid structures in which a judicious choice of the conditions is used to stack multiple shapes and sculpt continuously during the growth.

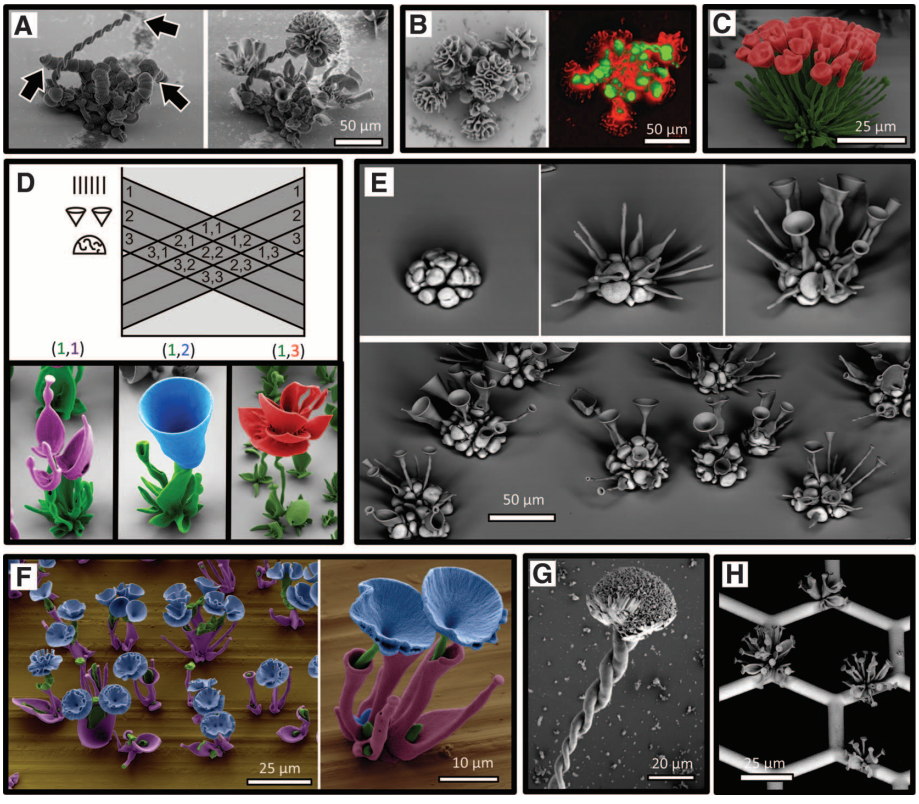

Fig. 5. Controlled synthesis of hierarchical complex structures. (**A** and **B**) $BaCO_3$-SiO_2 structures grown first in the solution containing fluorescein at pH 11.2 (regime 2) and then transferred to a solution containing rhodamine B at pH 11.8 (regime 1). Subsequent SEM images of the same structure (A) and confocal microscopy images (B) show that coral-like formations grow selectively on the active sites of the spirals [indicated by arrows in (A)], and no overgrowth occurs at the side walls of the previously formed shapes. (**C**) The SEM is false-colored, but represents the actual color of the structure composed of green $SrCO_3$-SiO_2 stems grown at pH 11.8 in the presence of fluorescein and then decorated with red, thick-walled $BaCO_3$-SiO_2 vases grown at 4°C in the presence of rhodamine B at pH 11.8. (**D**) Approach for making a combinatorial matrix of morphologies by changing the orientation of the substrate in distinct growth steps to stack different morphologies on top of each other. The SEMs of representative structures are false-colored to mark parts of the structure grown in different steps. (**E**) Multimaterial structure made in three steps: first, growing $BaCO_3$ corals that were thickened by addition of NaCl (top left) and, subsequently, inserting $SrCO_3$ stems (top center) and opening with a pulse of CO_2 (top right). The series is compiled from different structures. The bottom image is a large-area view. (**F**) False-colored SEMs showing a field of purple $SrCO_3$-SiO_2 vases containing $SrCO_3$-SiO_2 stems (green) that were subsequently opened with a CO_2 pulse (blue). (**G**) A spiral grown in regime 2 evolves into naked $BaCO_3$ crystals of regime 3 by lowering the pH of the bulk solution. (**H**) A transmission electron microscopy grid decorated with $SrCO_3$-SiO_2 stems that are opened with a CO_2 pulse. A larger variety of structures and overview images is provided in the supplementary materials (figs. S6 to S8).

Conclusions

Sequential modulations of environmental conditions such as pH, temperature, and CO_2 concentration are used to modify local chemical fields that directly influence the growth front and control directional structure evolution. We identify two distinct and complementary growth modes: (i) a "blossoming" regime, in which the structures grow away from each other and toward the bulk solution to form stems, vases, and corals; and (ii) a "curling" regime, in which the growing fronts tend to shield themselves from the bulk solution by curling back toward themselves and each other to form spiral and leaf structures. A detailed understanding of the underlying buffering mechanisms allows us not only to program these elementary shapes, but also to dynamically sculpt and pattern evolving structures and assemble them inside or on top of each other to generate hierarchically assembled multiscale architectures with unprecedented levels of complexity and precision.

References and Notes

1. P. Ball, *The Self-Made Tapestry* (Oxford Univ. Press, Oxford, 1999).
2. D. W. Thompson, *On Growth and Form* (Cambridge Univ. Press, Cambridge, 1917); abridged edition, J. T. Bonner, Ed. (1961).
3. P. Vukusic, J. R. Sambles, *Nature* **424**, 852 (2003).
4. K.-H. Chu, R. Xiao, E. N. Wang, *Nat. Mater.* **9**, 413 (2010).
5. J. Aizenberg *et al.*, *Science* **309**, 275 (2005).
6. J. K. Gansel *et al.*, *Science* **325**, 1513 (2009).
7. J. Ge, J. Lei, R. N. Zare, *Nat. Nanotechnol.* **7**, 428 (2012).
8. Z. Bao *et al.*, *Nature* **446**, 172 (2007).
9. B. Lim *et al.*, *Science* **324**, 1302 (2009).
10. M. J. Madou, *Fundamentals of Microfabrication: The Science of Miniaturization* (CRC Press, Boca Raton, FL, 2002).
11. G. M. Whitesides, B. Grzybowski, *Science* **295**, 2418 (2002).
12. H. A. Lowenstam, S. Weiner, *On Biomineralization* (Oxford Univ. Press, Oxford 1989).
13. P. Harting, *Q. J. Microsc. Sci.* **12**, 118 (1872).
14. J. J. Pagano, T. Bánsági Jr., O. Steinbock, *Angew. Chem. Int. Ed.* **47**, 9900 (2008).

15. J. H. E. Cartwright, J. M. García-Ruiz, M. L. Novella, F. Otálora, *J. Colloid Interface Sci.* **256**, 351 (2002).
16. C. Ritchie *et al.*, *Nat. Chem.* **1**, 47 (2009).
17. S. Mann, *Nature* **365**, 499 (1993).
18. S. Mann, G. A. Ozin, *Nature* **382**, 313 (1996).
19. G. Falini, S. Albeck, S. Weiner, L. Addadi, *Science* **271**, 67 (1996).
20. S. V. Patwardhan, S. J. Clarson, C. C. Perry, *Chem. Commun.* **2005**, 1113 (2005).
21. H. Y. Li, H. L. Xin, D. A. Muller, L. A. Estroff, *Science* **326**, 1244 (2009).
22. S.-H. Yu, H. Cölfen, K. Tauer, M. Antonietti, *Nat. Mater.* **4**, 51 (2005).
23. L. A. Gower, D. A. Tirrell, *J. Cryst. Growth* **191**, 153 (1998).
24. S. D. Sims, J. M. Didymus, S. Mann, *J. Chem. Soc. Chem. Commun.* **1995**, 1031 (1995).
25. J. M. García-Ruiz, E. Melero-García, S. T. Hyde, *Science* **323**, 362 (2009).
26. J. M. García-Ruiz, J. L. Amoros, *J. Cryst. Growth* **55**, 379 (1981).
27. J. M. García-Ruiz *et al.*, *Science* **302**, 1194 (2003).
28. M. Kellermeier *et al.*, *Chemistry* **18**, 2272 (2012).
29. T. Terada, S. Yamabi, H. Imai, *J. Cryst. Growth* **253**, 435 (2003).
30. H. C. Berg, E. coli *in Motion* (Springer, New York, 2003).
31. A. M. Turing, *Philos. Trans. R. Soc. London Ser. B* **237**, 37 (1952).
32. I. Lengyel, I. R. Epstein, *Science* **251**, 650 (1991).
33. G. Ertl, *Science* **254**, 1750 (1991).
34. S. Kondo, T. Miura, *Science* **329**, 1616 (2010).
35. G. M. Whitesides, R. F. Ismagilov, *Science* **284**, 89 (1999).
36. B. A. Grzybowski, *Chemistry in Motion* (Wiley, Chichester, 2009).
37. C. J. Brinker, G. W. Scherer, *Sol-Gel Science* (Academic Press, London, 1990).
38. W. L. Marshall, J. M. Warakomski, *Geochim. Cosmochim. Acta* **44**, 915 (1980).
39. Our hypothesis suggests that the bulk solution in regime 2 is above the optimum pH for silica formation, whereas in the vicinity of the growth front, the localized acid formation lowers the pH below the optimum level to precipitate silica on the active growth sites. We confirmed this localized pH gradient by monitoring $BaCO_3$-SiO_2 coprecipitation while deliberately adjusting the bulk pH (see supplementary materials).
40. We assume that the rate of the silica formation is slow enough to enter regime 2 before a layer of silica is formed that locks the coprecipitation in regime 1. We verified this assumption by starting from regime 2 and increasing the rate of silica precipitation by adding 0.2 mmol NaCl. As expected, we observe that the silica nucleation is now fast enough to not enter regime 2, but instead to grow thickened blossoming structures that correspond to regime 1.

Acknowledgments: We thank J. C. Weaver for advice with the SEM imaging, S. K. Y. Tang and R. Sadza for the microfluidic experiments, L. Hendriks for growing the structures in Fig. 5F, and A. J. Aizenberg for help with the manuscript. This work was supported by the NSF Materials Research Science and Engineering Centers under award no. DMR-0820484. W.L.N. thanks the Netherlands Organization for Scientific Research for financial support. EM was performed at Harvard's Center for Nanoscale Systems, supported by the NSF under award no. ECS-0335765.

Supplementary Materials

www.sciencemag.org/cgi/content/full/340/6134/832/DC1
Materials and Methods
Figs. S1 to S8

28 December 2012; accepted 19 March 2013
10.1126/science.1234621

Dual Molecular Signals Mediate the Bacterial Response to Outer-Membrane Stress

Santiago Lima,[1]* Monica S. Guo,[2]* Rachna Chaba,[3]† Carol A. Gross,[3,4] Robert T. Sauer[1]‡

In Gram-negative bacteria, outer-membrane integrity is essential for survival and is monitored by the σ^E stress-response system, which initiates damage-repair pathways. One activating signal is unassembled outer-membrane proteins. Using biochemical and genetic experiments in *Escherichia coli*, we found that off-pathway intermediates in lipopolysaccharide transport and assembly provided an additional required signal. These distinct signals, arising from disruptions in the transport and assembly of the major outer-membrane components, jointly determined the rate of proteolytic destruction of a negative regulator of the σ^E transcription factor, thereby modulating the expression of stress-response genes. This dual-signal system permits a rapid response to dysfunction in outer-membrane biogenesis, while buffering responses to transient fluctuations in individual components, and may represent a broad strategy for bacteria to monitor their interface with the environment.

The outer membrane (OM) is essential for the survival of Gram-negative bacteria. In *Escherichia coli*, the σ^E stress-response system recognizes signals indicative of OM dysfunction and triggers an adaptive response by activating the expression of gene products involved in the biogenesis, transport, and/or assembly of the lipopolysaccharides (LPSs), phospholipids, and outer-membrane proteins (OMPs) that make up the OM, and the proteases and chaperones that maintain or repair OM integrity (*1*, *2*). In this system, the RseA and RseB regulatory proteins and the DegS and RseP inner-membrane (IM) proteases transmit the signal that activates the σ^E transcription factor (fig. S1). RseA, a single-pass IM protein, has a cytoplasmic domain that binds and inhibits σ^E and a periplasmic domain ($RseA^P$) that binds RseB (*3*–*5*). After stress, OMPs accumulate in the periplasm, and their C-terminal

[1]Department of Biology, Massachusetts Institute of Technology, Cambridge, MA 02139, USA. [2]Department of Biochemistry and Biophysics, University of California, San Francisco, CA 94158, USA. [3]Department of Microbiology and Immunology, University of California, San Francisco, CA 94158, USA. [4]Department of Cell and Tissue Biology, University of California, San Francisco, CA 94158, USA.

*These authors contributed equally to this work.
†Present address: Indian Institute of Science Education and Research–Mohali, Sector 81, Knowledge City, S.A.S Nagar, Punjab 140306, India.
‡Corresponding author. E-mail: bobsauer@mit.edu

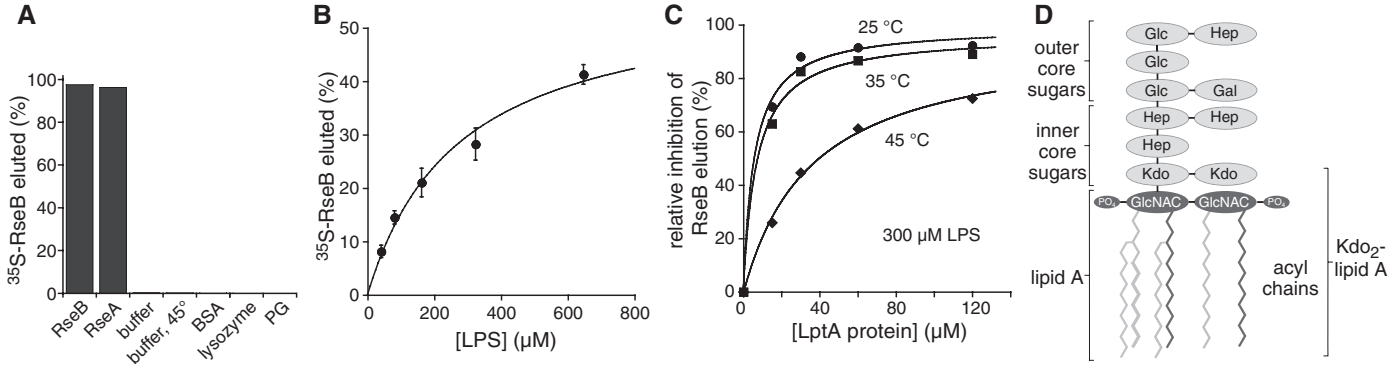

Fig. 1. LPS displaces RseA from RseB. (**A**) RseB (35 μM) and $RseA^P$ (100 μM) eluted ^{35}S-RseB (~1 μM) from $RseA^P$-agarose, whereas buffer controls, bovine serum albumin, (BSA, 125 μM), lysozyme (125 μM), or phosphatidylglycerol (PG, 13 mM) did not. (**B**) LPS from *E. coli* K12 eluted ^{35}S-RseB from $RseA^P$-agarose (25°C). Data (mean ± SD, $n = 3$ independent replicates) were fit to a hyperbolic function (K_{app} = 270 μM). (**C**) LptA inhibition of RseB elution by LPS (300 μM) was more efficient at lower temperatures. (**D**) Structure of *E. coli* K12 LPS (Kdo, keto-deoxyoctulosonate; Hep, heptose; Gal, galactose; Glc, glucose). The dark gray elements mediate RseB binding.